AWARD NUMBER: W81XWH-17-1-0503

TITLE: Constrictive Bronchiolitis in Previously Deployed Soldiers

PRINCIPAL INVESTIGATOR: Vasiliy Polosukhin, MD, PhD

CONTRACTING ORGANIZATION: Vanderbilt University Medical Center

REPORT DATE: October 2021

TYPE OF REPORT: Annual

PREPARED FOR: U.S. Army Medical Research and Development Command
Fort Detrick, Maryland 21702-5012

REPORT DOCUMENTATION PAGE

Form Approved
OMB No. 0704-0188

1. REPORT DATE	**2. REPORT TYPE**	**3. DATES COVERED**
OCTOBER 2021	Annual	09/15/2020-09/14/2021

4. TITLE AND SUBTITLE

Constrictive Bronchiolitis in Previously Deployed Soldiers

5a. CONTRACT NUMBER

5b. GRANT NUMBER
W81XWH-17-1-0503

5c. PROGRAM ELEMENT NUMBER

6. AUTHOR(S)
Vasiliy Polosukhin, MD, PhD

E-Mail: Vasiliy.v.polosukhin@vumc.org

5d. PROJECT NUMBER

5e. TASK NUMBER

5f. WORK UNIT NUMBER

7. PERFORMING ORGANIZATION NAME(S) AND ADDRESS(ES)
Vanderbilt University Medical Center
1161 21st Avenue,
Ste. D3300 MCN
Nashville, TN 37232-0011

8. PERFORMING ORGANIZATION REPORT NUMBER

9. SPONSORING / MONITORING AGENCY NAME(S) AND ADDRESS(ES)

U.S. Army Medical Research and Development Command
Fort Detrick, Maryland 21702-5012

10. SPONSOR/MONITOR'S ACRONYM(S)

11. SPONSOR/MONITOR'S REPORT NUMBER(S)

12. DISTRIBUTION / AVAILABILITY STATEMENT

Approved for Public Release; Distribution Unlimited

13. SUPPLEMENTARY NOTES

14. ABSTRACT We performed histopathological analysis of small airways (bronchioles) from 27 soldiers with constrictive bronchiolitis (CB), 55 patients with chronic obstructive pulmonary disease (COPD) and 18 non-diseased non-smoking (NS) controls. We found widespread pathological changes in COPD airways (loss of alveolar attachments, wall thickening and remodeling, decreased collagen density, and luminal occlusion by mucus plugs. Small airways of soldiers with CB were characterized by concentric fibrosis with increased collagen density and reduced elastin density without increase of wall thickness. These data provide reasonable explanation why soldiers with CB do not develop airway obstruction in spite of advanced fibrous remodeling in their small airways. Soldiers with CB also showed increased wall-to-lumen diameter ratio and small muscle hypertrophy in distal arterioles, collagen and elastin deposition and reduced density of blood capillaries in interalveolar septa, and thickening and fibrosis of pleura suggesting that pathological changes develop in all lung tissue compartments. We performed additional experiments in which we increased sulfur dioxide dose and found out that inhalation exposure (125 ppm) for 4 hours every day for 2 weeks is optimal. Based on similarity of pathological changes in exposed mice with those in soldiers with CB, we selected this model for future work.

15. SUBJECT TERMS Soldiers, constrictive bronchiolitis, small airways, airway inflammation, airway remodeling, airway epithelium, p73, polymeric immunoglobulin receptor, secretory IgA, mice, sulfur dioxide.

16. SECURITY CLASSIFICATION OF:			**17. LIMITATION OF ABSTRACT**	**18. NUMBER OF PAGES**	**19a. NAME OF RESPONSIBLE PERSON**
					USAMRMC
a. REPORT	**b. ABSTRACT**	**c. THIS PAGE**	Unclassified	**20**	**19b. TELEPHONE NUMBER** *(include area code)*
Unclassified	Unclassified	Unclassified			

TABLE OF CONTENTS

1. INTRODUCTION:

Constrictive bronchiolitis (CB) is a rare lung disease characterized by fibrotic remodeling of small airways. In 2011, King and colleagues reported that pathologic findings consistent with constrictive bronchiolitis (CB) were present in 38 active-duty military personnel presenting for evaluation for exertional dyspnea. All soldiers had previously been deployed to Afghanistan and/or Iraq as part of Operation Enduring Freedom or Operation Iraqi Freedom (OEF/OIF), and many of them reported exposure to the sulfur fire at the Mishraq State sulfur mine in June 2003. While certain inhalational exposures have previously been associated with CB, the mechanisms responsible for initiation and progression of the disease after inhalational injury are unknown. We hypothesize that exposure to airborne biohazards/toxins causes direct injury to the bronchiolar epithelium with loss of p73 expression, which is required for maintenance of the multi-ciliated cell (MCC) phenotype. Loss of MCCs leads to a reduction in pIgR, resulting in surface secretory IgA deficiency and a defective epithelial immune barrier that allows bacteria and inhaled antigens to drive persistent inflammation and fibrous remodeling of these small airways. To test our hypothesis, we propose the following specific aims: 1) to analyze the relationship between aberrant epithelial differentiation, loss of epithelial immune barrier function, and mural inflammation/remodeling in CB; and 2) to investigate sulfur dioxide inhalation as a model of CB in mice and test potential interventions. Our studies will investigate the novel concept that abnormal epithelial differentiation and impaired mucosal immunity underlie the pathogenesis of this disease, and will be among the first studies to investigate the role of p73 transcription factor in airway disease. In addition, our studies will characterize a new murine model of CB that can be used to investigate potential therapeutics for this important disease.

KEYWORDS

soldiers, constrictive bronchiolitis, small airways, airway inflammation, airway remodeling, airway epithelium, p73, polymeric immunoglobulin receptor, secretory IgA, mice, sulfur dioxide.

2. ACCOMPLISHMENTS:

What were the major goals of the project?

	Timeline (months)	**Percentage of completion**
Specific Aim 1: To analyze the relationship between aberrant epithelial differentiation, loss of epithelial immune barrier function and mural inflammation/remodeling in constrictive bronchiolitis.		
Local IRB approval: IRB approval is anticipated prior to or shortly after the beginning of the study period.	1-6	Approval received
Milestone(s) Achieved: USAMRMC Human Research Protection Office approval.	6	Approval received
Task 1: Evaluate lung samples from patients with constrictive bronchiolitis for epithelial structural changes, inflammation, and airway wall remodeling	1-18	
Subtask 1.1: Histological analysis of bronchiolar epithelial structural changes in constrictive bronchiolitis (e.g. immunohistochemical detection and count of ciliated cells, club cells and undifferentiated cells).		Complete
Subtask 1.2: Histological analysis of bronchiolar fibrous remodeling in constrictive bronchiolitis (e.g. quantitative measurements of wall thickening using histomorphometry technique).		Complete
Subtask 1.3: Histological analysis of bronchiolar inflammation in constrictive bronchiolitis (e.g. immunohistochemical detection and quantification of neutrophils, CD4, CD8 and CD19 lymphocytes).		Complete
Subtask 1.4: Protein isolation from frozen lung tissue samples and measurements of pro-inflammatory cytokines.		20%

Subtask 1.5: RNA isolation from frozen lung tissue samples and analysis of pro-inflammatory cytokine gene expression.		Complete
Milestone(s) Achieved: Evaluation of histopathological changes in individual bronchioles of soldiers with constrictive bronchiolitis, comparison analysis among study groups and data documentation.	18	90%
Task 2: Define epithelial immune barrier dysfunction in respiratory bronchioles in constrictive bronchiolitis	12-24	
Subtask 2.1: Detection and quantification of SIgA on surface of individual bronchioles in constrictive bronchiolitis (e.g. immunohistochemical detection and quantification of pIgR-positive ciliated cells in epithelial lining, direct measurement of IgA-specific immunofluorescence signal on mucosal surface of individual bronchioles).		Complete
Subtask 2.2: Detection and quantification of NF-κB signaling in bronchiolar epithelial cells (e.g. immunohistochemical detection and count of phospho-p65-positive cells).		Complete
Milestone(s) Achieved: Histological evaluation of mucosal immune disorders in individual bronchioles in constrictive bronchiolitis.	24	Complete
Task 3: Investigate bacterial invasion of the epithelial barrier in constrictive bronchiolitis.	18-36	
Subtask 3.1: Detection of bacterial species in individual bronchioles using *in situ* hybridization technique.		Complete
Subtask 3.2: DNA isolation from frozen lung samples and detailed analysis of lung microbiome using Respiratory Infections Microbial DNA qPCR Array.		Complete
Milestone(s) Achieved: Analysis of microbiome alterations in the lungs of soldiers with constrictive bronchiolitis (demonstration whether a more invasive or pro-inflammatory microbiome can be detected in the lungs of soldiers with constrictive bronchiolitis).	36	Complete
Specific Aim 2: To investigate sulfur dioxide inhalation as a model of constrictive bronchiolitis in mice and test potential interventions.		
Local IACUC approval: IACUC approval is anticipated prior to or shortly after the beginning of the study period.	1-3	Approval received
Milestone(s) Achieved: USAMRMC Animal Care and Use Review Office approval.	3	Approval received
Task 1: Optimizing our model of sulfur dioxide exposure (SO_2) to generate constrictive bronchiolitis. Total 96 mice will be used.	1-12	
Subtask 1.1: Mouse ordering and colony breeding.		Complete
Subtask 1.2: Inhalation exposure of mice to SO_2 using two different scheme: 1) single exposure to 125 ppm SO_2 for 4 hours and 2) repetitive exposures to 125 ppm SO_2 for 2 hours every other day for 1 week or 2 weeks.		Complete
Subtask 1.3: Analysis and quantification of fibrous remodeling in distal airways in mice after single or repetitive SO_2 inhalation exposure.		Complete

Subtask 1.4: Analysis of airway epithelial cell injury and regeneration/differentiation in mice after single or repetitive SO_2 inhalation exposure.		Complete
Subtask 1.5: Analysis of airway epithelial immune barrier dysfunction in mice after single or repetitive SO_2 inhalation exposure.		Complete
Subtask 1.6: Analysis of lung inflammation in mice after single or repetitive SO_2 inhalation exposure.		Complete
Subtask 1.7: Analysis of differences in lung microbiome in mice after single or repetitive SO_2 inhalation exposure.		0%
Milestone(s) Achieved: Evaluation of pathological changes in distal airways in mice after inhalation exposure to SO_2. Optimization of mouse model of constrictive bronchiolitis for future studies.	12	90%
Task 2: Time course study of airway pathology in mice after inhalation exposure to SO_2. Total 88 mice will be used.	12-24	
Subtask 2.1: Time course study (2, 4 or 6 months) for dynamic assessment of lung inflammation and airway fibrous remodeling in mice after inhalation exposure to SO_2. Total 48 mice will be used.		80%
Subtask 2.2: Time course study (48 hours, 1 week, 1 or 2 months) for analysis of ultrastructural manifestations of lung cell/tissue injury and airway fibrous remodeling developed in response to inhalation exposure to SO_2. Total 40 mice will be used.		80%
Milestone(s) Achieved: Dynamic analysis of histological and ultrastructural manifestations of pathological changes in distal airways in mice after inhalation exposure to SO_2.	24	80%
Task 3: Determining whether SO_2 exposure affects differentiation of ciliated cells *ex vivo*. Total 240 mice will be used.	6-24	
Subtask 3.1: Analysis of ability of tracheal epithelial cells to restore differentiation and structural specificity *ex vivo* after SO2 exposure.		0%
Subtask 3.2: Determining whether overexpression of p73 or FoxJ1 transcription factors can improve tracheal epithelial cell differentiation *ex vivo* after SO2 exposure.		0%
Milestone(s) Achieved: The role of transcription factors p73 and FoxJ1 in post-injurious regeneration and differentiation of airway epithelial cell will be investigated.	24	0%
Task 4: Interventions to prevent airway fibrosis in mice. Total 160 mice will be used.	25-36	
Subtask 4.1: Determining whether roflumilast intervention can prevent airway fibrosis in mice after SO2 inhalation exposure.		50%
Subtask 4.2: Determining whether antibiotics intervention can prevent airway fibrosis in mice after SO2 inhalation exposure.		50%

Milestone(s) Achieved: The test of hypothesis that anti-inflammatory treatments would be beneficial for lung inflammation and airway fibrosis.	36	50%

What was accomplished under these goals?

Specific Aim 1: To analyze the relationship between aberrant epithelial differentiation, loss of epithelial immune barrier function and mural inflammation/remodeling in constrictive bronchiolitis.

We have now completed a comprehensive histopathological analysis of the lungs of soldiers with constrictive bronchiolitis (CB). Details are described below.

Task 1: Evaluate lung samples from patients with constrictive bronchiolitis for epithelial structural changes, inflammation, and airway wall remodeling.

Subtask 1.1: Histological analysis of bronchiolar epithelial structural changes in constrictive bronchiolitis (e.g. immunohistochemical detection and count of ciliated cells, club cells and undifferentiated cells).

We detected a reduction of differentiated cells (ciliated, club and goblet cells) and the appearance of less differentiated bronchiolar epithelial cells in soldiers with CB compared to non-diseased (ND) control subjects (**Table 1**). These results suggest that incomplete cell differentiation persists in bronchiolar epithelium in soldiers with CB.

Table 1. Epithelial remodeling.

Parameters	**Non-diseased control subjects (N=17)**	**Soldiers with CD (N=27)**	**P value**
Ciliated cells (%)	84.6±5.0	61.4±13.2	p <0. 001
Club cells (%)	15.4±3.8	11.6±2.3	p < 0.01
Goblet cells (%)	1.2±1.1	0.9±1.7	p = 0.093

Subtask 1.2: Histological analysis of bronchiolar fibrous remodeling in constrictive bronchiolitis (e.g. quantitative measurements of wall thickening using histomorphometry technique).

We performed histological and morphometrical analysis of small airways (bronchioles that < 1 mm in diameter) from 50 soldiers with CB, 8 patients with sporadic CB, 21 patients with GOLD stages I-II COPD, 34 patients with GOLD stages III-IV COPD, and 17 ND controls in order to determine the factor(s) that drive airflow limitation. We assessed small airways for alveolar attachments to the surrounding lung parenchyma, wall remodeling/thickening, collagen/elastin density, and luminal mucus plugging. Small airways from COPD patients showed complex pathological changes including loss of alveolar attachments, wall thickening and remodeling, decreased collagen density, and frequent luminal occlusion by mucus plugs. Small airways of soldiers with CB were characterized by concentric fibrosis with increased collagen density and reduced elastin density without increase of wall thickness. Small airways of patients with sporadic CB were characterized by similar pathology (concentric fibrosis with increased collagen density and reduced elastin density) but with increase of wall thickness. Alveolar attachments and luminal mucus were similar between CB and NS airways (**Figures 1 and 2**). Since soldiers with CB do not develop airway obstruction, we postulated that isolated small airway pathology (fibrous remodeling) detected in their small airways is insufficient to cause significant airflow limitation; whereas, combined pathology (wall thickening, collagen scaffold degradation, loss of alveolar attachments and luminal mucus plugging) affects air flow through small airways in patients with COPD. Multivariable linear regression analysis revealed that loss of alveolar attachments is the major determinant of airflow limitation in COPD. Together, our data provide an explanation of why soldiers with CB do not have substantial airway obstruction in spite of fibrous remodeling in their small airways.

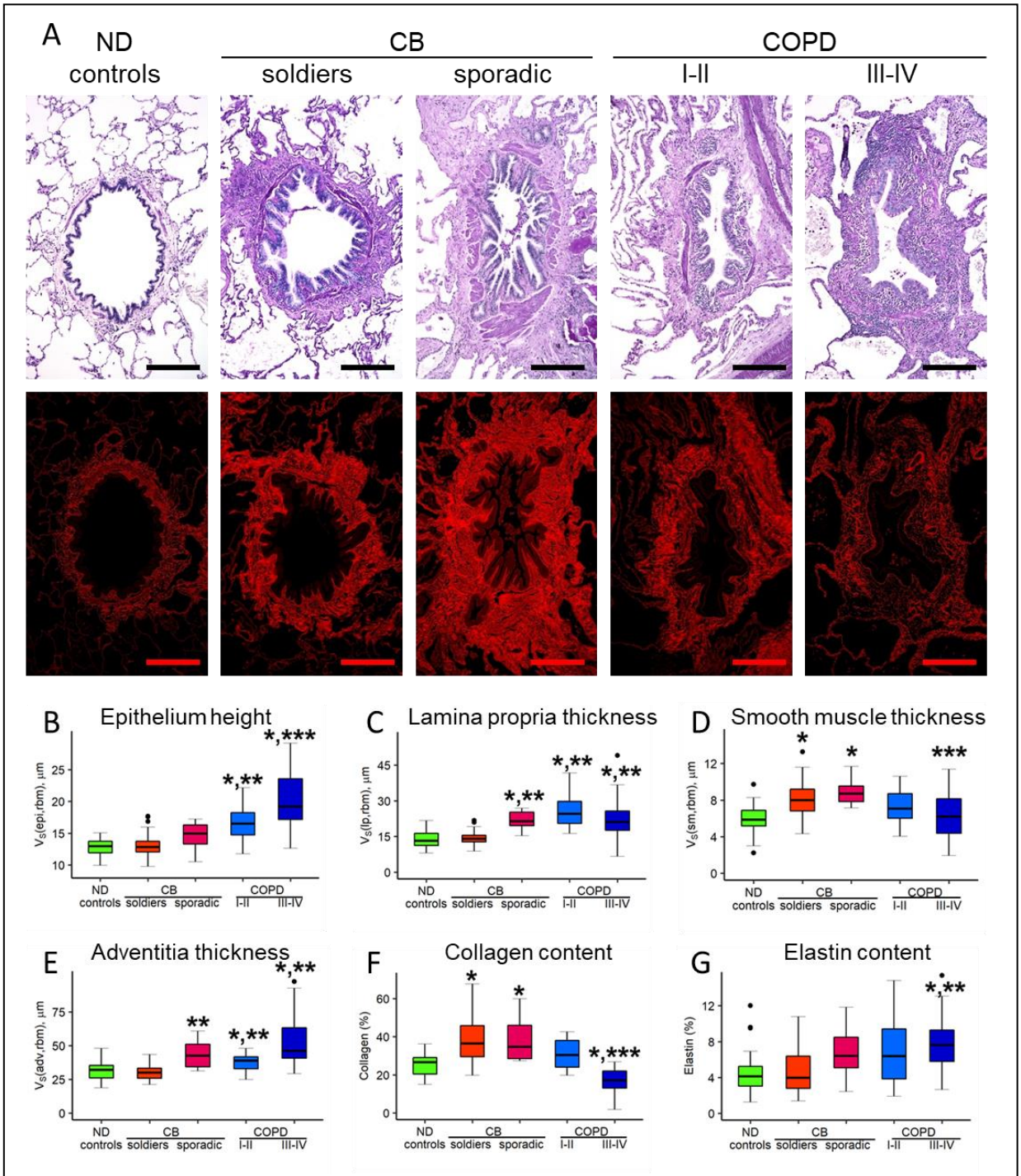

Figure 1. *Histomorphometric characteristics of small airways in CB and COPD*. A – representative small airways from ND control subject, soldier with CB, sporadic CB patient, GOLD I-II COPD patient, and GOLD III-IV COPD patient. Top row – periodic acid-Schiff (PAS) staining, bottom row – red fluorescence after PicroSirius red staining. Scale bars = 100 µm. B-G – box and whisker plots showing morphometric characteristics of small airway walls. Boxes represent the interquartile range, whiskers extend to the most extreme data point which is no more than 1.5 times the interquartile range from the box, and circles beyond the whiskers are extreme values, the line within the box represents the median. V_S(epi,rbm) – epithelial height, V_S(lp,rbm) – lamina propria thickness, V_S(sm,rbm) – smooth muscle layer thickness, V_S(adv,rbm) – adventitia thickness. Groups were compared pairwise using Mann-Whitney U test. P-values were Bonferroni-adjusted. The threshold for significance was 0.05. *significantly different compared to ND controls, **significantly different compared to soldiers with CB, *** significantly different compared to both soldiers with CB and sporadic CB groups.

To compare the immune/inflammatory phenotype in small airways from CB and COPD patients, we quantified lymphocytes and neutrophils, and the percent of small airways with associated tertiary lymphoid follicles (TLFs) on immunostained lung sections. Analysis of inflammatory cells in airway walls revealed an

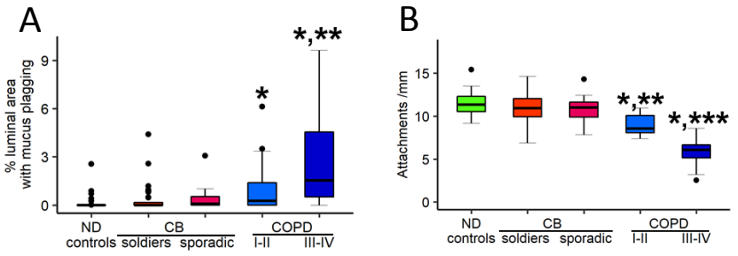

Figure 2. *Quantification of inner and outer small airway compartments in patients with CB and COPD*. A,B – box and whisker plots showing mucus plugging and number of alveolar attachments normalized to basal membrane length. Boxes represent the interquartile range, whiskers extend to the most extreme data point which is no more than 1.5 times the interquartile range from the box, and circles beyond the whiskers are extreme values, the line within the box represents the median. Groups were compared pairwise using Mann-Whitney U test. P-values were Bonferroni-adjusted. The threshold for significance was 0.05. *significantly different compared to ND controls, **significantly different compared to soldiers with CB, *** significantly different compared to both soldiers with CB and sporadic CB groups.

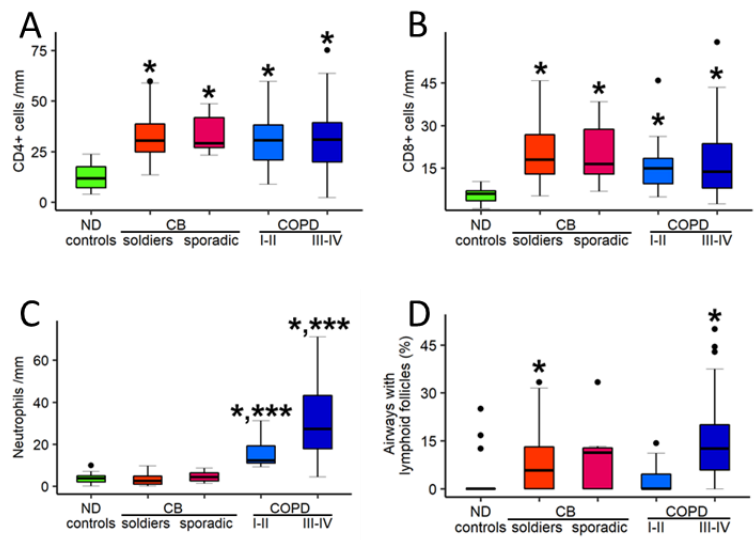

Figure 3. *Quantification of immune/inflammatory cells in small airways*. A-D – box and whisker plots showing presented $CD4^+$ and $CD8^+$ cells, neutrophils, and tertiary lymphoid follicles (TLFs). Boxes represent the interquartile range, whiskers extend to the most extreme data point which is no more than 1.5 times the interquartile range from the box, and circles beyond the whiskers are extreme values, the line within the box represents the median. Groups were compared pairwise using Mann-Whitney U test. P-values were Bonferroni-adjusted. The threshold for significance was 0.05. *significantly different compared to ND controls, **significantly different compared to soldiers with CB, *** significantly different compared to both soldiers with CB and sporadic CB groups.

influx of $CD4^+$ and $CD8^+$ T cells in both CB groups, and COPD patients. In contrast, neutrophils were increased in COPD but not CB patient airways (**Figure 3A-C**). Compared to ND controls, the percent of small airways with TLFs were significantly higher in soldiers with CB and patients with sporadic CB and GOLD Stage III-IV COPD, and trended to be higher in patients with sporadic CB (**Figure 3D**). Together, these findings suggest that persistent adaptive inflammation in small airways is characteristic of CB.

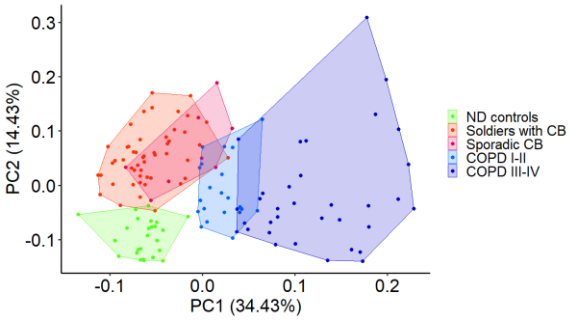

Figure 4. *Principal component analysis showing separation between groups of patients*. PC – principal components #1 and #2 with percent of explained diversity among measured components of small airway immunopathology.

To investigate the ability of histomorphometric parameters to separate patients with different diagnoses, we performed principal component analysis (PCA) based on all small airway morphometric parameters measured for all 138 study participants (**Figure 4**). This analysis revealed a clear separation of patients with CB (soldiers and sporadic) from ND controls and COPD patients. In addition, the analysis showed extensive overlap between soldiers with CB and sporadic CB, indicating important similarities between the two groups. In contrast, COPD patients were distinct from ND controls and CB patients, and GOLD stage III-IV patients had markedly different airway parameters compared to GOLD stage I-II patients. Further analysis showed that the principal component (PC) #1 explained diversity among patients based on a mixture of structural (primarily attachment loss and epithelial layer thickness) and inflammatory (neutrophil influx and lymphoid follicles) parameters, resulting in the clear separation of the two groups of COPD patients. The PC2 separated CB groups from ND controls primarily based on $CD4^+$ and $CD8^+$ T cell accumulation, smooth muscle thickness, and collagen deposition parameters. The relative contribution of individual small airway measurements to the first two PCA dimensions is presented in **Table 2**. A manuscript describing the airway changes in soldiers with CB, patients with sporadic CB and patients with COPD is currently submitted for publication.

Table 2. Relative contributions of small airway histopathological parameters to principal component (PC) analysis.

Small airway characteristic	PC1, %	PC2, %
V_S(epi,rbm), µm	13.9	2.8
V_S(lp,rbm), µm	8.0	0.0
V_S(sm,rbm), µm	0.6	13.4
V_S(adv,rbm), µm	12.2	0.0
Attachments/mm	15.9	0.6
Collagen (%)	10.2	5.3
Elastin (%)	4.0	0.7
Mucus (%)	10.7	0.2
CD8/mm	1.6	34.0
CD4/mm	1.0	33.0
Neutrophils/mm	15.8	0.0
Airways with follicles (%)	6.1	10.1

V_S(epi,rbm), epithelial height; V_S(lp,rbm), lamina propria thickness; V_S(sm,rbm), smooth muscle layer thickness; V_S(adv,rbm), adventitia thickness; /mm, values normalized by 1mm of reticular basement membrane length.

Next, in addition to analysis of small airway pathology, we undertook a comprehensive histomorphometric evaluation of blood vessels, interalveolar septa, and pleura in 50 affected soldiers and 17 non-diseased (ND) controls whose lungs were rejected for lung transplantation (**Table 3**). In bronchovascular bundles, pulmonary arterioles adjacent to small airways had a significant increase in medial thickness (due to smooth muscle hyperplasia/hypertrophy) in lungs of affected soldiers (**Figure 5 and Table 3**). Increased adventitial thickness due to edema and fibrosis was also identified in these arterioles. The combination of pathological changes in the media and adventitia of arterioles resulted in a marked increase in the wall-to-lumen ratio of these blood vessels (**Table 3**). In addition to pathological changes in arterioles adjacent to small airways, we observed remodeling of distal vasculature within the lung parenchyma. Muscularization and increased wall thickness were present in distal

Table 3. Morphometric evaluation of lung tissue samples.

Parameters	Non-diseased controls (N = 17)	Soldiers CB (N = 50)	P value
Inflammatory cells in airway wall			
CD4 cells (n/mm)	9.5 (6.2, 12.1)	30.4 (24.8, 38.6)	<0.001
CD8 cells (n/mm)	5.9 (3.5, 6.8)	17.9 (12.9, 26.8)	<0.001
Neutrophils (n/mm)	4.6 (3.1, 5.7)	2.5 (1.0, 4.8)	<0.05
Lymphoid follicles			
Adjacent to airways	2 (12%)	32 (64%)	<0.001
In alveolar tissue (*i.e*. beneath pleura)	1 (6%)	28 (56%)	<0.001
Both	0	22 (44%)	<0.001
Small airway walls			
Epithelial height ($V:SA_{EPI}$, µm)	13.2±1.1	13.1±1.8	0.70
Lamina propria thickness ($V:SA_{LP}$, µm)	12.4±2.5	14.3±2.8	<0.05
Smooth muscle thickness ($V:SA_{SM}$, µm)	6.1±1.8	8.0±1.9	<0.001
Adventitia thickness ($V:SA_{ADV}$) µm)	29.7±5.7	30.3±5.6	0.69
Collagen content (% of subepithelium)	26.6 (20.4, 28.6)	36.4 (29.5, 45.8)	<0.001
Elastin content (% of subepithelium)	3.87 (2.61, 5.14)	3.96 (2.79, 6.4)	0.57
Arterioles			
Smooth muscle thickness ($V:SA_{SM}$, µm)	19.9 (15.2, 20.7)	38.4 (31.7, 50.7)	<0.001
Adventitia thickness ($V:SA_{ADV}$, µm)	37.5 (33.7, 39.6)	47.9 (40.5, 59.3)	<0.001
Wall to internal diameter ratio	0.27 (0.22, 0.37)	0.44 (0.34, 0.61)	<0.001
Alveolar tissue (Inter-alveolar septa)			
Collagen content (LD_{COL}, µm)	1.1 (.97, 1.42)	2.0 (1.6, 2.3)	<0.001
Elastin content (LD_{ELAST}, µm)	0.7 (0.4, 0.8)	0.9 (0.8, 1.0)	<0.001
Blood capillary density (LD_{CAP}, n/mm)	69.4±3.9	61.1±5.2	<0.001
Pleura			
Thickening	0	23 (46%)	<0.001
Inflammatory cell infiltration	0	37 (54%)	<0.001
Fibrosis	0	44 (88%)	<0.001

Normally distributed numerical parameters are indicated as mean ± standard deviation; Non-normally distributed numerical parameters are indicated as median (interquartile range).

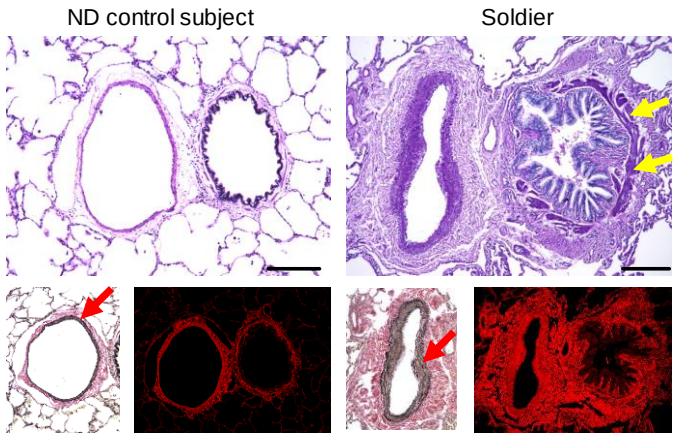

Figure 5. *Histopathology of bronchovascular bundles*. A – normal-appearing small airway and artery from ND control subject; small airway from soldier with moderate smooth muscle hypertrophy (yellow arrows), collagen deposition in subepithelium and constrictive-like luminal narrowing; pulmonary artery from soldier with increased medial thickness due to hypertrophy/hyperplasia of smooth muscle (red arrows). Top row – periodic acid-Schiff (PAS) staining, bottom row – left images demonstrate moderate smooth muscle hypertrophy in pulmonary artery in soldier (VVG staining); right images demonstrate increased collagen density in small airway and artery walls in soldier (collagen red fluorescence, PicroSirius red staining). Scale bars = 100 µm.

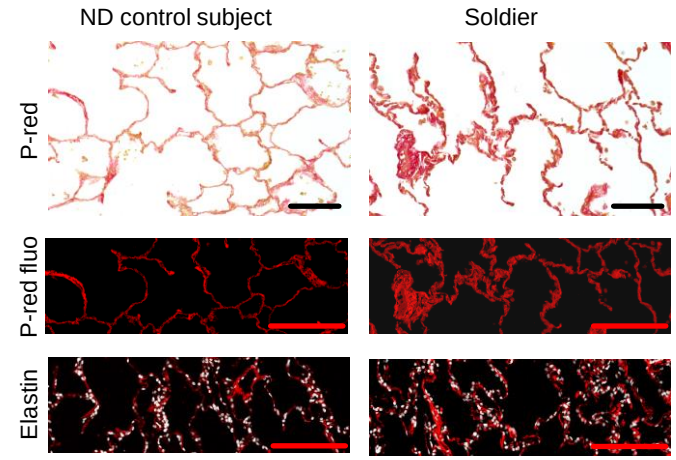

Figure 7. *Histopathology of alveolar tissue*. Top row images illustrate alveolar tissue of ND control subject and soldier (PicroSirius red staining, marked as P-red); middle row – collagen deposition in the IAS of soldier compared to ND control subject (red fluorescence after PicroSirius red staining, marked as P-red fluo); bottom row – elastin deposition in the IAS of soldier compared to ND control subject (red immunofluorescence). Scale bars = 50 µm.

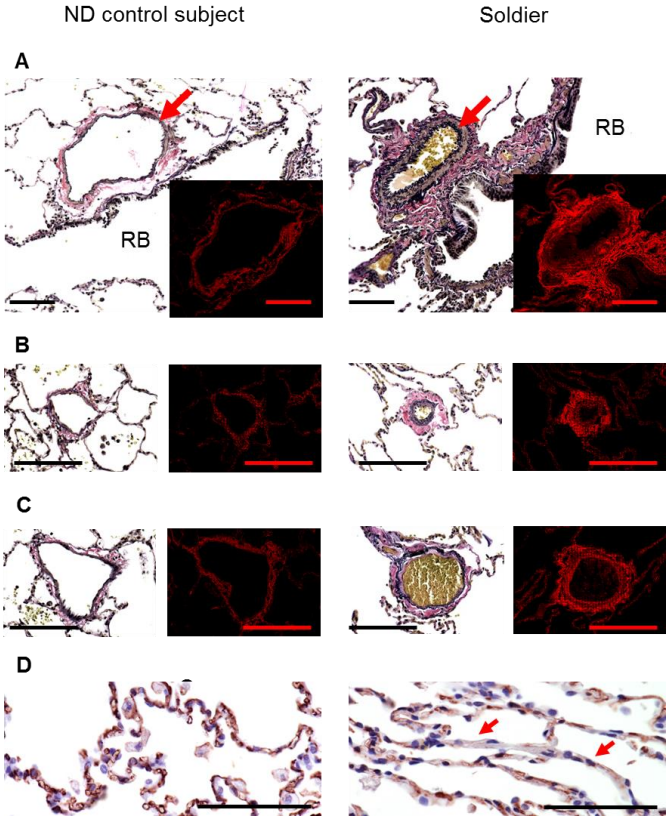

Figure 6. *Histopathology of distal vasculature*. A – muscularization of distal artery (red arrows) adjacent to respiratory bronchioles (RB) in soldier compared to ND control subject. VVG staining. B, C – increased wall thickness in post-capillary venule (B) and distal venule (C) due to excessive collagen deposition in adventitia in soldier compared to ND control subject. Distal blood vessels located within alveolar tissue and characterized by absence or indistinct internal elastic lamina were considered as pulmonary venules. Venules were considered as postcapillary venules if their size were < than surrounding alveoli or as distal venules if their size > than surrounding alveoli. A-C – left images represent VVG staining; right inserts/images demonstrate collagen red fluorescence on PicroSirius red staining. D – blood capillaries in IAS in ND control subject and loss of blood capillaries in some IAS (red arrows) in soldier. CD31 immunostaining. Scale bars = 50 um.

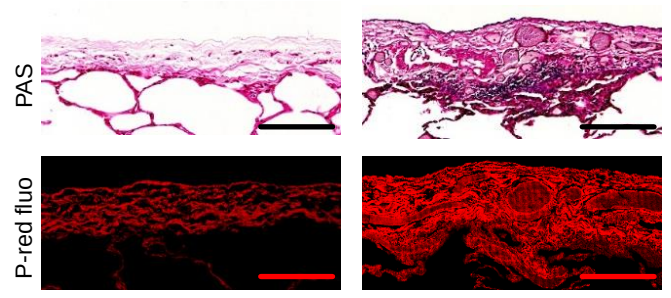

Figure 8. *Histopathology of visceral pleura*. Top row images illustrate thickening and inflammation of visceral pleura soldier compared to ND control subject (PAS staining); bottom row – collagen deposition in the pleura of soldier compared to ND control subject (red fluorescence after PicroSirius red staining, marked as P-red fluo). Scale bars = 50 µm.

arteries adjacent to respiratory bronchioles (**Figure 6A**).

In the alveolar compartment, we identified increased wall thickness of distal venules with collagen deposition in the adventitia (**Figures 6B and 6C**). Evaluation of the interalveolar septa (IAS) revealed a reduction in blood capillary density in lungs of affected soldiers (**Figure 6D and Table 3**). In addition, the IAS in affected soldiers showed a diffuse fibrotic phenotype with increased deposits of collagen and elastin, but without distortion of alveolar architecture (**Figure 7, Table 3**).

Pathologic changes of visceral pleura, which were not observed in ND controls, were present in 92% of affected soldiers (**Figure 8, Table 3**). Pleural pathology was characterized by: 1) infiltration of mononuclear

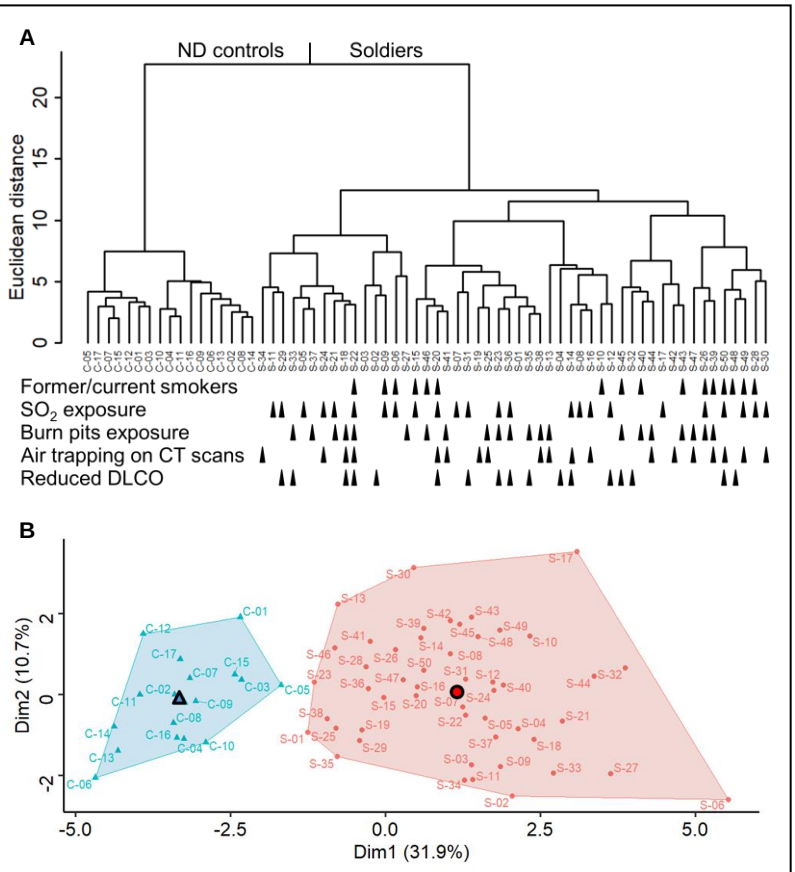

Figure 9. *Unsupervised hierarchical clustering analysis shows separation of affected soldiers and control subjects*. A – Unsupervised Hierarchical Clustering Dendrogram using Euclidean distance metric for clustering and calculating the similarity between two clusters with Ward's method. Red borders separate 2 sub-clusters within soldier's cluster. B – 2D plot where points represent individual subjects according to the two principal components that explain the majority of the variance.

inflammatory cells (mostly lymphocytes) within and beneath the pleural lining (54% of affected soldiers), 2) pleural thickening (46% of affected soldiers), and/or 3) collagen deposition (fibrosis) identified on PicroSirius red staining (88% of affected soldiers).

To investigate whether pathological findings in the lungs could effectively separate diseased soldiers from ND controls, we performed unsupervised hierarchical clustering based on morphometric parameters. This analysis showed complete separation of these 2 groups (**Figure 9A**). Further analysis showed that the optimal number of clusters was 2, indicating a relatively homogeneous disease group (**Figure 9B**). Using LASSO logistic regression analysis, we identified parameters with the most discriminatory power for separating symptomatic soldiers from ND controls. These included: 1) CD4 and CD8 T cell infiltration of small airway walls, 2) medial thickness in pulmonary arterioles, 3) reduced density of blood capillaries in IAS, and 4) pleura pathology. Cumulatively, these parameters were sufficient to completely separate the two groups, suggesting that persistent immune cell infiltration, along with pathological changes in blood vessels and pleura, are conserved aspects of lung pathology in affected soldiers.

These findings have been published in American Journal of Surgical Pathology.

Subtask 1.3: Histological analysis of bronchiolar inflammation in constrictive bronchiolitis (e.g. immunohistochemical detection and quantification of neutrophils, CD4, CD8 and CD19 lymphocytes).

A striking finding in bronchioles of affected soldiers was a >3-fold increase in CD4 and CD8 T cells within the airway walls (**Table 2**). In contrast, no increase in neutrophils was observed in affected soldiers compared to ND controls. In addition to lymphocytic inflammation within the airway walls, we observed lymphoid follicles in close proximity to small airways in 64% of soldiers and within alveolar tissue in 56% of soldiers (**Table 2**). For comparison, lymphoid follicles were rarely present in ND control lungs (12% had lymphoid follicles adjacent to small airways and 6% within alveolar tissue). Further, diffuse infiltration of CD4 and CD8 T cells was observed in lung parenchyma and pleura from affected soldiers. Together, these findings indicate that adaptive immune activation is a prominent feature of lung pathology in affected soldiers.

Subtask 1.4: Protein isolation from frozen lung tissue samples and measurements of pro-inflammatory cytokines.

We isolated proteins from available lung tissue samples from patients with COPD and non-diseased NS controls. This preliminary work is necessary to establish protocol for future studies.

Subtask 1.5: RNA isolation from frozen lung tissue samples and analysis of pro-inflammatory cytokine gene expression.

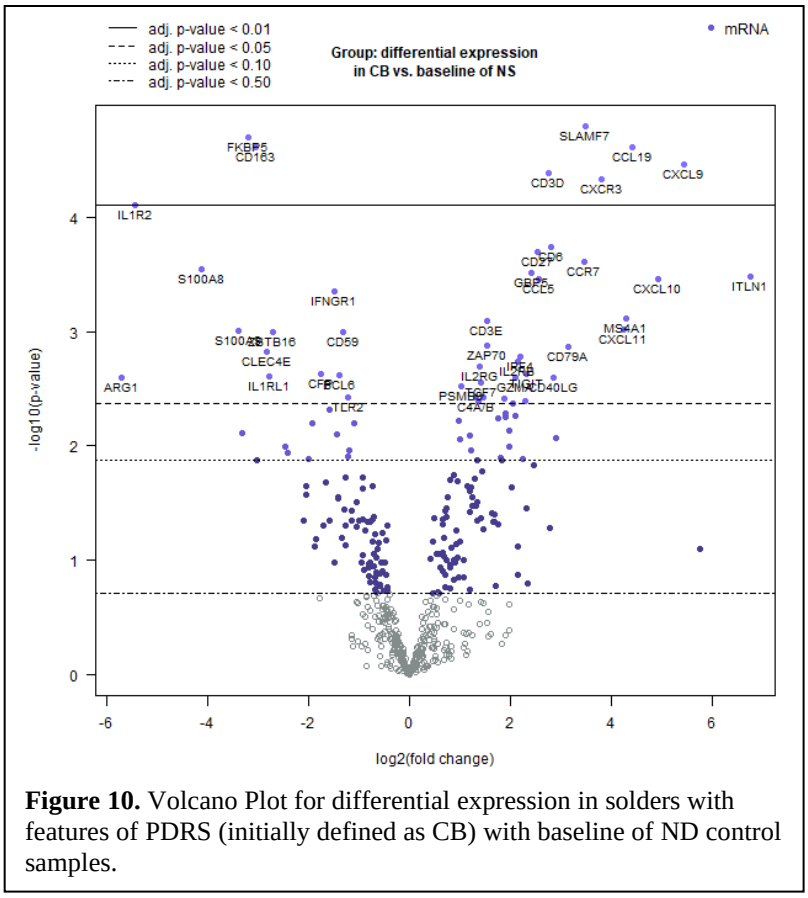

Figure 10. Volcano Plot for differential expression in solders with features of PDRS (initially defined as CB) with baseline of ND control samples.

We isolated RNA from 8 soldiers with CB and 4 non-diseased controls. For RNA expression analysis, we used nCounter® Immunology Panel (NanoString Technologies, WA). The panel is based on a novel digital molecular barcoding technology (PlexSet Technology) that allows to count directly the RNA molecules. With this panel, we performed multiplex gene expression analysis for 579 immune inflammatory genes and 15 internal reference genes. This panel includes major classes of cytokines and their receptors, enzymes with specific gene families such as the major chemokine ligands and receptors, interferons and their receptors, the TNF-receptor superfamily, and the KIR family genes. 84 genes involved with the anti-fungal immune response are also included.

The differential expression analysis in soldier's samples compared to ND controls with Benjamini-Hochberg (BH) p-adjustment revealed 45 genes with at least 2-fold change in expression (**Figure 10**).

The Reactome Project analysis revealed up-regulation of genes responsible for:

1. adaptive immune pathways including B Cell Receptor (BCR)-signaling, T Cell Receptor (TCR)-signaling, immunoregulatory interactions between Lymphoid and non-Lymphoid cells, co-stimulation by the CD28 family;
2. cytokine signaling including TNFR2 non-canonical NF-kB pathway, Interleukin-2 family signaling and Interleukin-3, Interleukin-5 and GM-CSF signaling, interferon gamma signaling;
3. RAF/MAP kinase cascade;
4. signal transduction including signaling by GPCR, signaling by WNT, regulation of KIT signaling.

In contrast, genes participating in innate immune response associated pathways such as Toll-like Receptor cascades, neutrophil degranulation, TRAF6 mediated NF-kB activation, complement cascade, antimicrobial peptides, advanced glycosylation end product receptor signaling are down-regulated.

In addition, genes participated in following pathways are down-regulated:

1. Interleukin-1 family signaling;
2. signal transduction including signaling by Rho GTPases;
3. gene expression (transcription) including TP53 Regulates Transcription of Cell Death Genes, FOXO-mediated transcription of cell death genes, MECP2 regulates neuronal receptors and channels from RNA Polymerase II Transcription.

Milestone(s) Achieved: **Task 1** has been largely completed. Our findings indicate that beyond CB, affected soldiers have pathological changes in all distal lung compartments. Based on these findings, it is clear that the previous report that focused on pathological changes in small airways underestimated the nature and extent of lung pathological remodeling in this cohort of affected soldiers. Therefore, we propose ***post-deployment respiratory syndrome*** (PDRS) as a better descriptor for the combination of: 1) history of deployment in Iraq and Afghanistan, 2) inhalational exposures during deployment, 3) chronic respiratory symptoms (exertional dyspnea and reduced exercise tolerance) that develop in the post-deployment period, and 4) lung pathology that affects all distal lung compartments. Persistent accumulation of lymphocytes suggests an ongoing local activation of adaptive immunity. This work is paradigm shifting by showing that environmental exposures can cause diffuse

and persistent pathological changes in the distal lung. The combined effects of this lung pathology may account for the severe and persistent symptoms experienced by these soldiers.

Task 2: Define epithelial immune barrier dysfunction in respiratory bronchioles in constrictive bronchiolitis.

Subtask 2.1: Detection and quantification of SIgA on surface of individual bronchioles in CB (e.g. immunohistochemical detection and quantification of pIgR-positive ciliated cells in epithelial lining, direct measurement of IgA-specific immunofluorescence signal on mucosal surface of individual bronchioles).

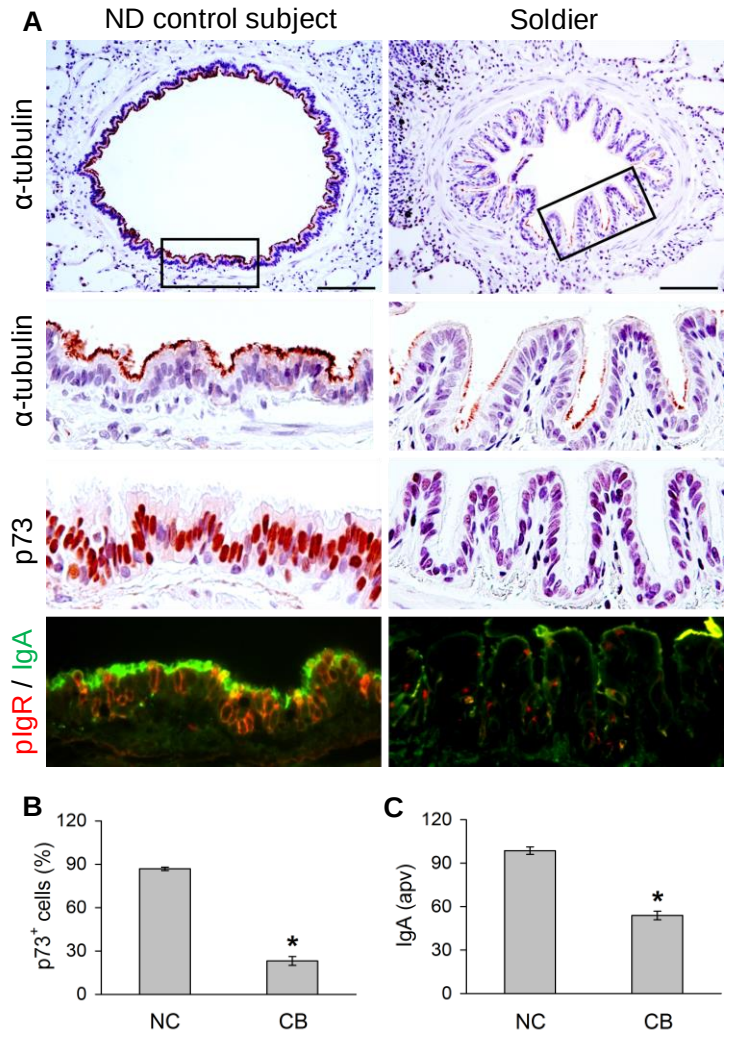

Figure 11. *Loss of differentiated ciliated cells in bronchioles of soldiers with constrictive bronchiolitis is associated with reduced p73 expression and SIgA deficiency on the bronchiolar surface*. A – immunostaining for α-tubulin, p73, and IgA/pIgR on serial tissue sections. Scale bars = 100 μm. Black boxes indicate inserts. B – percentage of p73 expressing epithelial cells. C – IgA immunofluorescence levels on the airway surface measured as actual pixel value (apv) for each bronchiole. Mean ± SEM. *=p<0.01.

We have measured IgA-specific immunofluorescence on the epithelial surface of bronchioles from 28 soldiers with PDRS (initially defined as CB) and 17 ND controls. Significant reduction of IgA immunofluorescence was detected on mucosal surface of bronchioles of soldiers suggesting mucosal SIgA deficiency. We also found reduced p73 expression in bronchilar epithelial cells in soldiers with PDRS compared to ND controls (**Figure 11**).

Subtask 2.2: Detection and quantification of NF-κB signaling in bronchiolar epithelial cells (e.g. immunohistochemical detection and count of phospho-p65-positive cells).

Quantification of NF-κB signaling in bronchiolar epithelial cells did not reveal significant changes of p65 expression in bronchiolar epithelial cells in soldiers compared to ND controls.

Milestone(s) Achieved: **Task 2** has been completed. Our findings show that SIgA deficiency in soldiers with PDRS (initially defined as CB) is associated with incomplete epithelial cell differentiation in bronchiolar epithelium. These results further support our hypothesis that epithelial alterations and immune barrier dysfunction play a role in disease pathogenesis in affected soldiers.

Task 3: Investigate bacterial invasion of the epithelial barrier in constrictive bronchiolitis.

Subtask 3.1: Detection of bacterial species in individual bronchioles using *in situ* hybridization technique.

This analysis has been performed for 28 soldiers with PDRS (initially defined as CB) and 17 ND control subjects. Bacterial species were detected by *in situ* hybridization technique using a probe for the bacterial gene encoding 16S ribosomal RNA (rRNA). Compared to ND controls, bronchioles in soldiers were frequently infected by bacterial species – 9.3 (0-16.7) 5 vs. 0 (0-0) % (p<0.001).

Subtask 3.2: DNA isolation from frozen lung samples and detailed analysis of lung microbiome using Respiratory Infections Microbial DNA qPCR Array.

This study was aimed to determine whether lung microbiome in soldiers with PDRS (initially defined as CB) is characterized by an appearance of more invasive (or pro-inflammatory) microbial species compared to normal subjects. To address this issue, we analyzed bacterial DNA extracted from lung tissue samples obtained from 8 soldiers and 8 non-diseased control subjects. DNA was analyzed by the Respiratory Infections Microbial DNA qPCR Array (Qiagen). This array contains assays for 41 respiratory bacterial species including *Haemophilus influenzae, Moraxella catarrhalis and Pseudomonas aeruginosa.* Our study did not show any pathogenic respiratory bacterial species in both soldiers with CB and non-diseased control subjects.

Milestone(s) Achieved: These studies indicate that loss of ciliated cells in individual bronchioles from soldiers with PDRS (initially defined as CB) is accompanied by reduced SIgA on the airway surface, chronic intrapulmonary lymphocytic inflammation, and diffuse pathological changes affecting small airways, pulmonary vasculature, alveolar tissue and visceral pleura.

Specific Aim 2: To investigate sulfur dioxide inhalation as a model of constrictive bronchiolitis in mice and test potential interventions.

To date, we have:
1) Established mouse model of PDRS (initially defined as CB).
2) Performed histological and morphometrical analysis of mouse lung specimens.

Task 1: Optimizing our model of sulfur dioxide exposure (SO_2) to generate constrictive bronchiolitis.

Subtasks 1.2-1.6:

To develop a model of PDRS (initially defined as CB) in mice, we reasoned that SO_2 could be an appropriate stimulus given the reported exposure to this toxin by soldiers with PDRS. We treated male and female wild-type (WT) mice (C57BL/6J background, 8-10 weeks of age) with inhalational exposure of 125 ppm SO_2 for 4 hours (x1 SO_2) because this level of SO_2 was reported in areas where soldiers with PDRS were positioned during deployment. We selected 4-hours exposure because this time period was found to be optimal in a series of pilot experiments. We harvested mouse lungs at 36 hours, 14 days, or 28 days after exposure for evaluation. We found sloughing of the lining epithelium in large airways and evidence of injury and edema of lining epithelium in small airways at 36 hours, as well as hemorrhage and inflammation in the lung parenchyma (not shown). Although the epithelium of small airways was restored by 14 day after exposure to SO_2, the lining epithelial cells appeared abnormal. The α-tubulin staining at 14 and 28 days after SO_2 exposure showed a marked reduction in multi-ciliated cells (MCCs) at both time points, suggesting that acute, severe injury to the epithelial lining can lead to long-term impairment in epithelial differentiation (**Figure 12**).

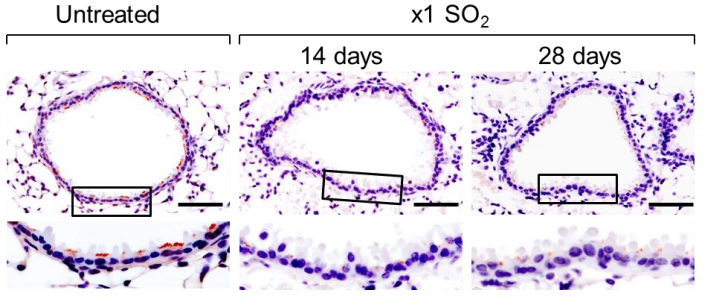

Figure 12. *Persistent loss of MCCs in small airways from mice exposed to SO_2.* Immunostaining with antibody for α-tubulin. Scale bars = 50 μm.

Then we performed experiments with increased SO_2 exposure. We found that inhalation of 125 ppm for 4 hours a day, 1 day per week for 3 weeks (x3 SO_2 scheme) or for 4 hours a day, 5 days per week for 2 weeks (x10 SO_2 scheme) was optimal to develop a PDRS-like phenotype in affected mice. Pathological changes in SO_2 exposed mice were detected in all distal lung compartments and included lymphocytic inflammation, airway and vascular remodeling, and collagen deposition within IAS and visceral pleura.

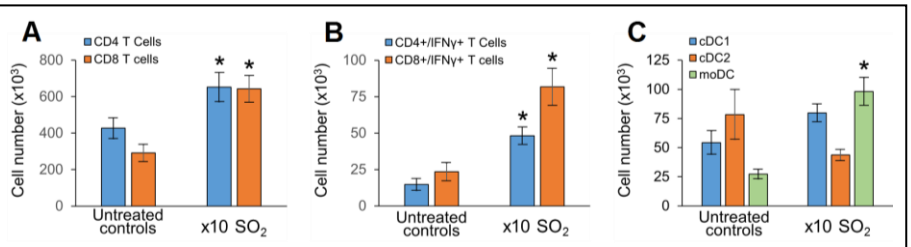

Figure 13. *Quantification of intrapulmonary immune cells*. Increased numbers of CD4 and CD8 T cells (A), $CD4^+$/Interferon-γ^+ and $CD8^+$/Interferon-γ^+ T cells (B), and monocyte-derived dendritic cells (C) in SO_2 exposed mice compared to unexposed age-matched mice. * - $p<0.05$ compared to unexposed mice. Data presented as mean ± SE. N = 8 mice per study group.

To analyze immune inflammatory cells in SO_2-exposed mice, we made single cell suspensions from lungs of untreated control mice and mice 28 days after repetitive SO_2 exposure (x10 SO_2). Analysis of lymphocyte subsets by flow cytometry showed that T cells (both CD4 and CD8 and their subtypes) were increased in exposed mice, suggesting adaptive immune activation that similar to PDRS. We also measured type 1 and type 2 conventional and monocyte-derived dendritic cells (cDC1, cDC2, and moDC) and found no difference in number of cDC1 and cDC2 but increased moDC in SO_2-exposed mice (**Figure 13**).

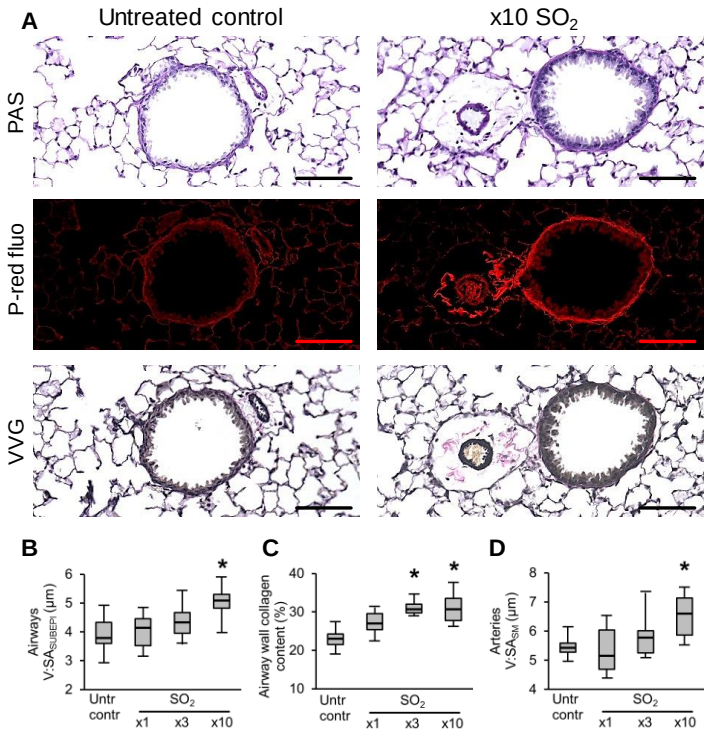

Figure 14. *Inhalation exposure to SO_2*. A – normal-appearing bronchovascular bundle in untreated WT mice; progressive increased wall thickness and collagen deposition in distal small airways; medial thickness and edema and fibrosis of adventitia in pulmonary artery in WT mice exposed to repetitive SO_2. Scale bars = 50 μm. B and C – graphs showing increased collagen content deposition (B) in distal small airways and increased media thickness (C) in mice exposed to SO_2. * - $p<0.05$ compared to unexposed mice. N = 6 mice per study group.

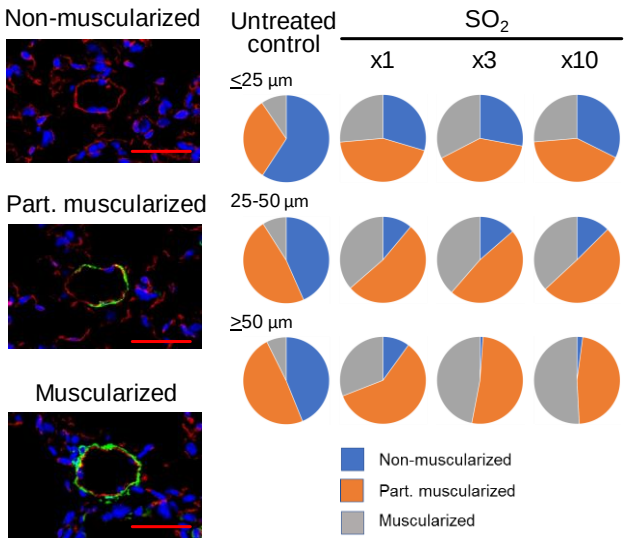

Figure 15. *SO_2 inhalation exposure induces abnormal muscularization in distal intra-acinar blood vessels*. Images illustrate examples of non-muscularized, partially muscularized (≤50% vessel circumference with smooth muscle) and muscularized (>50% vessel circumference with smooth muscle) blood vessels with size 25-50 μm. Double immunofluorescence with anti-CD31 (red) and anti-α-smooth muscle actin (green) antibodies. Scale bars = 25 μm. 2D Pie charts illustrate distribution of non-muscularized, partially muscularized and muscularized intra-acinar blood vessels in untreated and repetitively exposed to SO_2 mice. $p < 0.01$ for each study group compared to untreated control mice by Chi-square test. N = 6 mice per study group.

Further analysis showed that repetitive inhalation exposure of mice to SO_2 resulted in more prominent lung pathology than a single treatment at 28 days post-exposure. It is important to note that pathology was largely observed in the bronchovascular bundles (i.e. - the lung parenchyma did not display substantial inflammation or emphysematous changes). **Figure 14** displays prominent small airway fibrosis and increased medial thickness in adjacent pulmonary arteries in mice exposed to repetitive SO_2 compared to untreated or singe exposed mice. In addition, abnormal muscularization of distal intra-acinar vessels was detected in exposed mice (**Figure 15**) with degree similar to other PH murine models.

In addition to small airways and blood vessel remodeling, mice exposed to SO_2 showed progressive dose-dependent diffuse fibrosis of alveolar tissue and visceral pleura (**Figure 16**). At the same time, significant architectural distortions that are usually associated with pulmonary fibrosis were not noticed.

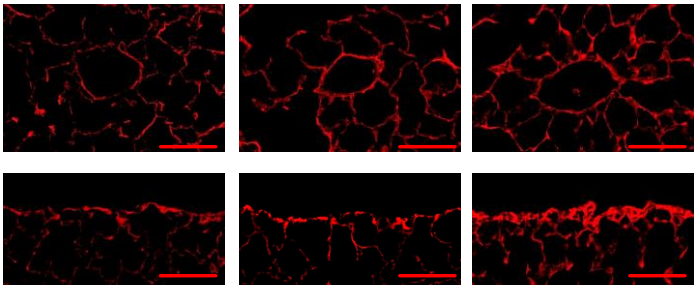

Figure 16. *SO_2 inhalation exposure induces diffuse fibrosis in alveolar tissue and visceral pleura*. Progressive collagen deposition in IAS and blood vessel wall (top row) and in visceral pleura (bottom row) in mice exposed to single and repetitive SO_2. Red fluorescence after PicroSirius red staining, marked as P-red fluo. Scale bars = 25 µm.

Milestone(s) Achieved: These studies are largely complete and indicate that: 1) mice exposed to SO_2 recapitulate general manifestation of PDRS (initially defined as CB). We found that mice exposed to SO_2 were characterized by: 1) reduction of differentiated ciliated cells in airway epithelium; 2) significant reduction of pIgR expression in airway epithelial cells and surface SIgA deficiency on epithelial (mucosal) surface; 3) increased frequency of bacterial colonization; 4) persistent intrapulmonary inflammatory cell infiltrations (mostly CD4 and CD8 T cells); 5) airway wall fibrous remodeling (increased wall thickness excessive collagen accumulation).

Task 2: Time course study of airway pathology in mice after inhalation exposure to SO_2.

Subtask 2.1: Time course study (2, 4 or 6 months) for dynamic assessment of lung inflammation and airway fibrous remodeling in mice after inhalation exposure to SO_2.

In these experiments, 8 mice per time point, including both male and female mice, were exposed to SO_2 (125 ppm for 4 hours every day for 2 weeks) and harvested at 2, 4, and 6 months after the initial exposure. Age-matched mice exposed to filtered air were used as a control. Lung tissue samples have been collected, processed and archived. Dynamic evaluations of lung inflammation and airway fibrous remodeling will be done during the last year period.

Subtask 2.2: Time course study (48 hours, 1 week, 1 or 2 months) for analysis of ultrastructural manifestations of lung cell/tissue injury and airway fibrous remodeling developed in response to inhalation exposure to SO_2.

To investigate ultrastructural abnormalities, we selected single SO_2 exposure (125 ppm for 4 hours). Mice were exposed to SO_2 (or filtered air) and lungs were harvested at different time points after SO_2 exposure - 48 hours (acute injury), 1 week (early recovery), 1 or 2 months (established pathological changes). Lung tissue samples have been collected, processed and archived. Dynamic evaluation of ultrastructural manifestations of lung cell/tissue injury and airway fibrous remodeling will be done during the last year period.

Task 3: Determining whether SO_2 exposure affects differentiation of ciliated cells *ex vivo*.

These studies have not been performed yet and will be completed during the last year period.

Task 4: Interventions to prevent airway fibrosis in mice.

Both experiments with roflumilast and antibiotic interventions are done. Lung tissue samples have been collected, processed and archived. Analysis will be done during the last year period.

4. IMPACT:

What was the impact on the development of the principal discipline(s) of the project?

Persistent exertional dyspnea in soldiers deployed to Southwest Asia is an emerging health problem that has been attributed to constrictive bronchiolitis. However, based on initial evaluation of lung samples from these patients, we performed a comprehensive histomorphmetric evaluation of lung biopsies, including evaluation of small airways, pulmonary vasculature, alveoli, and visceral pleura. In affected soldiers, we identified diffuse lung pathology characterized by lymphocytic inflammation, fibrosis of small airways, lung parenchyma, and pleura, and hypertensive-type vascular remodeling. Based on our findings, it is clear that the previous focus on pathological changes in bronchioles vastly underestimates the nature and extent of lung pathological remodeling in affected soldiers. Therefore, we propose post-deployment respiratory syndrome (PDRS) as a better descriptor for the combination of: 1) history of deployment in

Southwest Asia and Afghanistan, 2) inhalational exposures during deployment, 3) chronic respiratory symptoms (reduced exercise tolerance and exertional dyspnea) that persist in the post-deployment period and are not explained by standard diagnoses, and 4) lung pathology as described above that affects all distal lung compartments. This work is paradigm shifting by showing that environmental exposures can cause diffuse and persistent pathological changes in the distal lung. The combined effects of this lung pathology may account for the severe and persistent symptoms experienced by these soldiers.

In addition to evaluation of pathology in human lungs, other studies have characterized a new murine model of PDRS that can be used to investigate potential therapeutics for this important disease.

What was the impact on other disciplines?

Nothing to report.

What was the impact on technology transfer?

Nothing to report.

What was the impact on society beyond science and technology?

Nothing to report.

5. CHANGES/PROBLEMS:

Actual or anticipated problems or delays and actions or plans to resolve them

Soldiers with post-deployment PDRS (initially defined as CB) and exertional dyspnea develop pathological changes not only in small airways (as we initially proposed) but also in other lung tissue compartments, including pulmonary vasculature, alveolar tissue, and pleura. Therefore, we decided to perform additional histological and morphometrical analyses beyond the planned evaluation of small airways.

Changes that had a significant impact on expenditures

Nothing to report.

Significant changes in use or care of human subjects, vertebrate animals, biohazards, and/or select agents

Nothing to report.

Significant changes in use or care of human subjects

Nothing to report.

Significant changes in use or care of vertebrate animals

Nothing to report.

Significant changes in use of biohazards and/or select agents

Nothing to report.

6. PRODUCTS:

- **Publications, conference papers, and presentations**

Abstract presented:

1) Comparative Histological and Morphometrical Analysis of Small Conducting Airways in Constrictive Bronchiolitis and COPD. American Thoracic Society 2018 International Conference, San Diego, CA.
2) Comparative Histological and Morphometrical Analysis of Small Conducting Airways in Constrictive Bronchiolitis and COPD. The Thomas L Petty Aspen Lung Conference 2018, Aspen, CO.
3) The Histopathological Basis of Airflow Limitation in Small Airways Disease. American Thoracic Society 2019 International Conference, Dallas, TX.
4) Mucosal Immune Disorders in Small Airways Disease. International Congress of Mucosal Immunology 2019, Brisbane, Australia.
5) Small Airway Pathology in Constrictive Bronchiolitis and Chronic Obstructive Pulmonary Disease. American Thoracic Society 2021 International Conference.

- **Journal publications.**

Published:

1) Richmond BW, Mansouri S, Serezani A, Novitskiy S, Blackburn JB, Du RH, Fuseini H, Gutor S, Han W, Schaff J, Vasiukov G, Xin MK, Newcomb DC, Jin L, Blackwell TS, Polosukhin VV. Monocyte-derived dendritic cells link localized secretory IgA deficiency to adaptive immune activation in COPD. *Mucosal Immunol.* 2021, 14(2):431-442.
2) Polosukhin VV, Gutor SS, Du RH, Richmond BW, Massion PP, Wu P, Cates JM, Sandler KL, Rennard SI, Blackwell TS. Small airway determinants of airflow limitation in chronic obstructive pulmonary disease. *Thorax*, 2021 (Online ahead of print).
3) Gutor SS, Richmond BW, Du R-H, Wu P, Sandler K.L., MacKinnon G., Brittain EL, Lee JW, Ware LB, Loyd JE, Johnson JE, Miller RF, Newman JH, Rennard SI, Blackwell TS, Polosukhin VV. Post-deployment respiratory syndrome in soldiers with chronic exertional dyspnea. *Am J Surg Pathol*, 2021 (Online ahead of print).

Submitted for publication:

1) Gutor SS, Richmond BW, Du RH , Wu P, Lee JW , Ware LB , Shaver CM , Novitskiy SV, Johnson JE, Newman JH, Rennard SI, Miller RF, Blackwell TS, Polosukhin VV. Characterization of Immunopathology and Small Airway Remodeling in Constrictive Bronchiolitis.

Additional planned manuscripts include: 1) manuscript describing small airway mucosal immunopathology in soldiers with PDRS, 2) manuscript describing mouse model of SO_2 induced lung pathology, 3) review article.

- **Books or other non-periodical, one-time publications.** N/A
- **Other publications, conference papers and presentations**. N/A
- **Website(s) or other Internet site(s).** N/A
- **Technologies or techniques.** N/A
- **Inventions, patent applications, and/or licenses.** N/A
- **Other Products.** N/A

7. PARTICIPANTS & OTHER COLLABORATING ORGANIZATIONS
What individuals have worked on the project?

Name: Vasiliy V. Polosukhin, M.D., Ph.D.
Project Role: P.I.
Research Identifier (e.g. ORCID ID): 0000-0001-9845-8041
Nearest person month worked: 1.0

Contribution to project: Dr. Dr. Polosukhin is the PI and has performed completion of the work proposed, experiment planning, interpreting and trouble-shooting, and facilitated interactions among investigators.
Funding support: N/A

Name: Sergey S. Gutor, Ph.D.
Project Role: Postdoctoral
Research Fellow
Research Identifier (e.g. ORCID ID): 0000-0003-4402-0516
Nearest person month worked: 11.2
Contribution to project: Dr. Gutor performs histopathological and morphometrical examination of human and mouse lung tissue samples with the oversight of Dr. Polosukhin.
Funding support: N/A

- **Has there been a change in the active other support of the pd/pi(s) or senior/key personnel since the last reporting period?**

Other Support Changes:

Timothy S. Blackwell, M.D.
New: VUMC89082 (Blackwell)
Ended: R01HL131906 (Blackwell)

Vasiliy V. Polosukhin, M.D., Ph.D.
New: R01HL157373 (Benjamin); R01HL157583 (Dikalov); R01HL122554 (Newcomb)
Ended:

- **What other organizations were involved as partners?**

Nothing to report.

8. SPECIAL REPORTING REQUIREMENTS

- **COLLABORATIVE AWARDS:** N/A
- **QUAD CHARTS:** N/A

9. APPENDICES: N/A